ACS APPLIED MATERIALS & INTERFACES

Research Article

www.acsami.org

Microwave-Assisted Synthesis of Porous Carbon–Titania and Highly Crystalline Titania Nanostructures

Alison Parker,[†] Michal Marszewski, and Mietek Jaroniec*

Department of Chemistry and Biochemistry, Kent State University, Kent, Ohio 44242, United States

Supporting Information

ABSTRACT: Porous carbon–titania and highly crystalline titania nanostructured materials were obtained through a microwave-assisted one-pot synthesis. Resorcinol and formaldehyde were used as carbon precursors, triblock copolymer Pluronic F127 as a stabilizing agent, and titanium isopropoxide as a titania precursor. This microwave-assisted one-pot synthesis involved formation of carbon spheres according to the recently modified Stöber method followed by hydrolysis and condensation of titania precursor. This method afforded carbon–titania composite materials containing anatase phase with specific surface areas as high as 390 m^2 g^{-1}. The pure nanostructured titania, obtained after removal of carbon through calcination of the composite material in air, was shown to be the anatase phase with considerably higher degree of crystallinity and the specific surface area as high as 130 m^2 g^{-1}. The resulting titania, because of its high surface area, well-developed porosity, and high crystallinity, is of great interest for catalysis, water treatment, lithium batteries, and other energy-related applications.

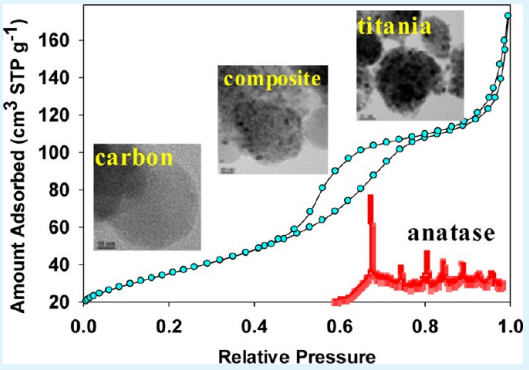

KEYWORDS: *carbon spheres, carbon–titania composites, crystalline titania, porous materials, anatase, microwave-assisted synthesis*

1. INTRODUCTION

Nanoparticles, because of their unique physical and chemical properties that stem from their size in the nanometer range, incur great attention from researchers and scientists among different science disciplines.[1] Titanium dioxide (TiO_2, titania), among other photoactive materials, is intensively investigated because of its projected feasibility in photocatalysis and other photo-related applications.[2−4] Titania materials are also widely employed in the fields of films and coatings,[5] lithium-ion batteries,[6] dye-sensitized solar cells,[7] medicine,[8] and even in food and personal care.[9] In addition to these applications, titania is an important material because of its high stability, non-toxicity, abundance, and low production and processing cost.[10,11] TiO_2 properties can be altered via chemical modifications such as doping and grafting, or other processes such as hydrothermal treatment, which can generate structural and morphological changes.[12] Moreover, TiO_2 can be used to form composite nanostructures to achieve the desired properties for specific catalytic and photocatalytic applications.[11]

Numerous studies of carbon–titania composite nanostructures such as spheres,[13−17] rods,[14,18] and ordered mesoporous materials[19] showed the enhanced effectiveness of those materials in energy storage,[20,21] water treatment,[22] and catalysis.[23] Ao et al.[13] prepared C-TiO_2 core–shell particles by coating TiO_2 onto carbon spheres using titanium butoxide under neutral, non-aqueous conditions. Later, the spheres were calcined in air atmosphere to produce hollow spheres of TiO_2, which were ca. 300 nm in diameter and 50 nm in thickness. The obtained TiO_2 nanostructures contained anatase phase and showed superior photocatalytic activity toward degradation of methylene blue as compared to the reference material Degussa P25. Subsequently, Zheng et al.[14] proposed a general protocol for coating TiO_2 on carbon nanostructures. According to their procedure, ammonia is used to introduce basic conditions during the coating process and, therefore, to better match interactions between carbon surface and titania precursors. It was shown that the method could be used to coat TiO_2 on carbon spheres, rods, and even carbon composite materials containing silver or iron oxide. Most recently, Li et al.[15] showed that this coating procedure could be extended to other nanostructures. By precise controlling of kinetics of the coating process the authors were able to form TiO_2 layers on α-Fe_2O_3 ellipsoids, Fe_3O_4 spheres, SiO_2 spheres, graphene oxide nanosheets, and carbon nanospheres. Zhuang et al.[16] prepared hollow composite microspheres and hollow titania microspheres with good photocatalytic properties and specific surface areas of 105 and 94 m^2 g^{-1}, respectively. Shi et al.[17] used the established protocol to obtain C-TiO_2 core–shell nanostructures and showed that by careful thermal treatment it is possible to introduce C-doping and enhance the visible-light photoactivity of the resulting titania hollow spheres. These hollow microspheres showed over sixfold better performance toward degradation of methyl orange as compared to Degussa P25; however, their specific surface area was small (41 m^2 g^{-1}).

Received: November 13, 2012
Accepted: February 22, 2013
Published: February 22, 2013

Wu et al.[18] synthesized C-doped titania nanotubes, nanorods, and nanowires with high specific surface areas; however, those materials contained different crystalline phases such as anatase and rutile. Liu et al.[19] showed that the soft-templating strategy, employing Pluronic F127 copolymer as a structure-directing agent, is a good method for producing ordered mesoporous carbon−titania composites with very high specific surface area, controllable composition, and good photocatalytic activity. Hexagonally ordered mesoporous carbon−titania materials had exceptionally high specific surface area in the range of 209 − 465 m^2 g^{-1}, pore volume in the range of 0.16−0.26 cm^3 g^{-1}, and mesopore width ca. 4.1 nm; however, those structural parameters decreased significantly with increasing content of titania, and the value of the specific surface area for pure TiO_2 material was not reported. Moreover, this method has a limited ability to greatly vary the pore size of the resulting composites. The above literature survey shows the importance of carbon−titania composite materials and outlines the challenges remaining to be solved. While the synthesis of various carbon−titania composites has been achieved, there is still room for improvement of their morphological properties. The aforementioned limitations in the synthesis of both carbon−titania composites and highly crystalline titania structures with tunable morphology and porosity provided inspiration for the current study. Here, we explore the use of microwaves for the synthesis of carbon−titania composite nanostructures to achieve the desired morphology, pure anatase phase, high specific surface area, and narrow pore-size distribution of these materials. Hsu et al.[24] synthesized the flower-like mixed-phase titania nanostructures under microwave conditions; this group was able to produce materials very similar in size and properties to the samples prepared using traditional oven heating. Later, Jia et al.[25] demonstrated that the microwave irradiation can play an important role in maintaining the morphology of titania nanorods during calcination at high temperatures.

The current work, building upon previous studies, reports the microwave-assisted synthesis of porous carbon−titania composites and highly crystalline titania nanostructures. A one-pot procedure as opposed to the multi-step processes used in previous works was employed to obtain the aforementioned composites. The previously modified Stöber method for the synthesis of carbon spheres[26] was chosen as a starting point and further modified through the use of temperature-programmed microwave technique.[27] Deposition of TiO_2 was carried out through hydrolysis and condensation of titanium isopropoxide. Basic conditions were used to better match interactions between carbon materials and titania precursor. The use of microwave is beneficial because it allows for programming and screening the synthesis conditions over a wide range of temperature and time, which creates additional opportunities in controlling the morphology, porosity, and surface area of the resulting materials. An additional advantage of the proposed synthesis is the ability to remove carbon from the composite, used mainly for the protection of titania structure during thermal treatments, to finally produce highly crystalline porous titania with large specific surface area and well-developed and tuned porosity.

2. EXPERIMENTAL SECTION

2.1. Materials. Resorcinol (1,3-dihydroxybenzene, $C_6H_4(OH)_2$), 37% (w/w) formaldehyde (HCHO) solution stabilized with 10−15 % methanol, and 98+% titanium(IV) isopropoxide (TIPO) were purchased from Acros Organics. Triblock copolymer Pluronic F127 was donated by BASF, USA. The 30% (w/w) ammonia (aqueous solution) was purchased from Fischer Scientific. Ethanol used was technical grade. Deionized water was used throughout.

2.2. Preparation of Porous Carbon−Titania Nanostructured Materials. In a typical synthesis of carbon−titania composites, varying amounts of triblock copolymer Pluronic F127 (see Table 1 for more details) and 0.20 g of resorcinol were dissolved in 8 mL of ethanol and 20 mL of water to form a clear solution. After approximately 5 minutes, 0.1 mL of 30% (w/w) ammonia was added under stirring. In a 5 min interval, 0.28 mL of 37% (w/w) formaldehyde was added dropwise. The solution was allowed to stir for another 5 min (all together 15 min), was then transferred to a microwave (MW) Teflon container, and was subjected to a two-stage MW treatment. All MW programs utilized vigorous stirring and a 5 min ramp to the target temperature. The first stage was a two-step temperature program with initial step at 30 °C and the second step at 100 °C. Subsequently, in the second stage, after vessels were allowed to cool to 60−65 °C, the resulting red solution was supplied with 20 mL of ethanol and varying amounts of TIPO. The solution was then allowed to stir for 5 min, and then vessels were returned to MW for an additional 2 h at 100 °C. Finally, after cooling to 55−65 °C, the solution was transferred to a Petri dish and dried at 60 °C overnight. The obtained materials were transferred in quartz boats into a tube furnace for carbonization in nitrogen atmosphere. The heating program was as follows: first, temperature was ramped from room temperature to 350 °C with a 1 °C min^{-1} heating rate and dwelled for 2 h; next, temperature was ramped to 600 °C with a 1 °C min^{-1} heating rate and dwelled for 4 h; finally, the samples were allowed to cool down to room temperature. The obtained samples were denoted as CS-T-2.5 and CS*-T-0.7; Table 1 lists details of MW temperature program and amounts of polymer and titania precursor used during the synthesis.

Table 1. Synthesis Conditions of the Carbon−Titania Composite Materials

sample	polymer amount (g)	time at 30 °C (h)	time at 100° C (h)	TIPO (mL)
CS-T-2.5	0.50	6	12	2.5
CS*-T-0.7	0.20	15	15	0.7

As a reference, pure carbon materials, denoted as CS and CS*, were synthesized using the above procedure. The samples were obtained with the same amounts of polymer and heating program in MW as well as during carbonization; however, they did not undergo the addition of TIPO or additional ethanol.

2.3. Preparation of Highly Crystalline Titania Nanostructured Materials. Highly crystalline titania nanostructured materials were prepared from carbon−titania composite materials obtained in the previous section by removal of carbon under heating in air atmosphere. Briefly, the carbon−titania composites were transferred in quartz boats into a tube furnace for calcination in air atmosphere. The heating program was as follows: first, temperature was ramped from room temperature to 550 °C with a 1 °C min^{-1} heating rate and dwelled for 4 h; then, the samples were allowed to cool down to room temperature.

2.4. Characterization. Nitrogen adsorption−desorption isotherms were measured at −196 °C using a volumetric analyzer ASAP 2010 manufactured by Micrometrics, Inc. (Norcross, GA, USA). Prior to an adsorption measurement, each sample was outgassed at 200 °C for 2 h.

Transmission electron microscopy (TEM) images were taken using a 200 kV FEI Tecnai F20 TEM equipped with a field emission gun. The energy dispersive X-ray spectroscopy (EDX) data were obtained with the integrated scanning TEM (STEM) unit and attached EDAX spectrometer. *Z* (atomic number)-contrast images were acquired using a high-angle angular dark field (HAADF) detector with a spatial resolution < 1 nm. The samples for TEM were first suspended in ethanol, and then a droplet of the sample was placed on a carbon-coated copper TEM grid (400 mesh). TEM specimens were allowed to air dry and were kept in vacuum for a few hours to minimize the contamination during the TEM observation.

Scanning electron microscopy (SEM) images were taken using Hitachi Tabletop Microscope TM-1000 operated at 15 kV accelerating voltage and Hitachi High-Resolution SEM microscope S-4300 operated at 5 kV accelerating voltage.

High-resolution thermogravimetric measurements were conducted using a TA Instruments TGA Q500 (New Castle, DE, USA) thermogravimetric analyzer. TG and DTG curves were recorded from 25 to 800 °C in flowing air with a heating rate of 10 °C min^{-1}.

Wide-angle powder X-ray diffraction (WAXRD) spectra were measured using Cu Kα radiation on an X-ray diffractometer X'Pert PRO manufactured by PANalytical Inc. (Westborough, MA, USA). WAXRD spectra were collected in the continuous scan mode in the range of 2θ values from 10.00° to 80.00° with the step size 0.02° and the time-per-step 1.5 s (scan speed 0.013°/s).

Microwave-assisted synthesis was performed using a MARS 5 Microwave System manufactured by CEM Corporation (Matthews, NC, USA).

2.5. Calculations. Low-temperature nitrogen physisorption data was used to calculate the structural parameters of the obtained materials. A linear form of the Brunauer–Emmett–Teller (BET) equation[28] was used to estimate the monolayer capacity from adsorption data in the range of relative pressures from 0.05 to 0.2, which after conversion to the number of molecules per gram and multiplication by the cross-sectional area of nitrogen molecule gives the specific surface area, S_{BET}, of the sample studied.[29,30] Nitrogen cross-section area was assumed to be 0.162 nm^2/molecule.[30] Total pore volume, V_t, was calculated based on adsorption value at relative pressure p/p_0 = 0.99, converted to the volume of liquid nitrogen at −196 °C (measurement temperature).[29] Pore size distribution was calculated by employing the Barrett–Joyner–Halenda (BJH) procedure[31] using the relation between the pore width and relative pressure established on the basis of adsorption data for a series of MCM-41 materials used as model adsorbents.[32] The statistical film thickness curve was selected to be either obtained for Cabot BP280 carbon black material[33] in the case of carbon particles and composite materials or LiChrospher Si-1000 silica material[34] in the case of pure titania materials. Micropore volume, V_{mi}, was calculated by integration of the PSD curve up to 2.5 nm; since by definition the micropores have sizes below 2 nm, the aforementioned value contains a contribution from small mesopores. Mesopore volume, V_{me}, was calculated by subtraction of the micropore volume from the total pore volume. Micropore size, w_{mi}, was estimated from the position of the PSD maximum in range of micropores. Mesopore size, w_{me}, was estimated from the position of the PSD maximum in the mesopore range. Relative crystallinity of the composite materials was established using PANalytical X'Pert HighScore software version 2.1 by adjusting the background constant so that the corresponding pure titania material was ideally crystalline.

3. RESULTS AND DISCUSSION

Two series of carbon spheres, carbon–titania composites and their corresponding pure titania materials, were synthesized. Transmission electron microscopy (TEM) and scanning electron microscopy (SEM) were used to investigate the structure and morphology of the obtained materials at nanoscale level. Figure 1 shows TEM images of CS and CS* carbon particles. Both materials exhibit roughly spherical morphology with visible agglomeration between the particles. The average diameter of the particles is 39 ± 6 nm for CS and 53 ± 7 nm for CS* material, as estimated by analysis of images. The difference in the particle size is triggered by different amounts of the block copolymer used during the synthesis. The polymer acts as stabilizing agent during the growth of particles and, therefore, has impact on their final size.[26,35] The amounts of polymer used were selected to obtain carbon particles in a sub-100 nm range. The latter is beneficial from a structural viewpoint as smaller particles provide higher values of the specific surface area, as well as the mesopore volume, created due to their agglomeration (further discussed in the following section).

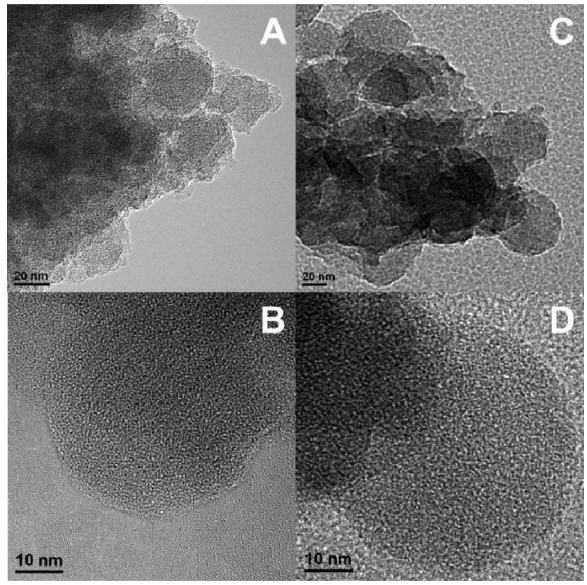

Figure 1. TEM images of carbon particles: CS material (A and B), CS* material (C and D).

Figure 2 shows TEM images of the composite materials studied. As can be seen in this figure, titanium dioxide is present in the form of small nanocrystals (6–10 nm in diameter), agglomerated on a scaffold of carbon particles. The resulting nanostructured titania shells are larger for CS-T-2.5 than those for CS*-T-0.7, due to higher amount of titania precursor added during the synthesis. Energy-dispersive X-ray spectroscopy (EDS/EDX) proved the presence of carbon and titania in those materials (spectra not shown). SEM images (Supprting Information Figure S1) of CS*-T-0.7 show a highly porous nature of the material (panel A) along with spherical morphology of carbon–titania structures (panel B). The

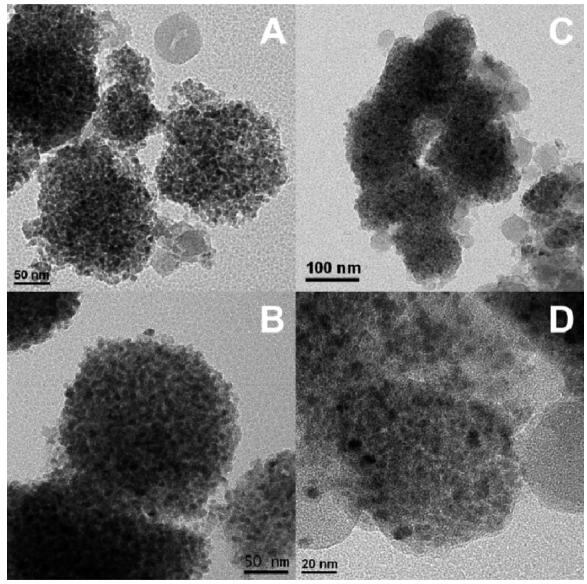

Figure 2. TEM images of carbon–titania composite materials: CS-T-2.5 material (A and B), CS*-T-0.7 material (C and D).

former is particularly suitable for the targeted applications, namely, electrodes in Li-based batteries, water treatment, and catalysis; as in all of these applications porosity facilitates transport of mater to and from the surface of material.

Pure titania materials, obtained after carbon removal, partially retain morphology of the composite materials (Supprting Information Figures S2 and S3). As can be seen in these figures, in the case of T-2.5 material, agglomeration of titania nanocrystals increases after carbon removal. In contrast, T*-0.7 material seems to retain the structure casted by the carbon spheres. In the case of both materials, the crystallite size of TiO_2 increased noticeably (10−20 nm in diameter) as compared to the composite materials. On the basis of Z-contrast STEM images (panel D in Supprting Information Figures S2 and S3) one can notice that hollow shells of titania crystals are created after removal of carbon cores; however, their presence is more pronounced for T*-0.7 material, which is understandable if one takes into account a much higher amount of titania in T-2.5 as compared to T*-0.7 that would require much more carbon for its protection during thermal treatments.

Low-temperature nitrogen adsorption measurements were conducted to further investigate structural and textural properties of the composite materials. Table 2 contains the adsorption parameters for all samples studied, calculated by using methods briefly described in the Experimental Section. Figure 3 shows nitrogen adsorption−desorption isotherms for a set of CS, CS-T-2.5, and T-2.5 samples, along with their pore size distribution functions (PSD, inset in Figure 3). Changes in the shape of consecutive isotherms reflect changes in the structural and adsorption properties of the materials after titania introduction and subsequent carbon removal. After deposition of TiO_2 on the micro−mesoporous carbon material consisting of carbon spheres (CS), a reduction in the structural parameters is observed. The specific surface area changes from 590 $m^2\ g^{-1}$ for CS to 240 $m^2\ g^{-1}$ for CS-T-2.5, and the porosity changes from 0.39 $cm^3\ g^{-1}$ for CS to 0.25 $cm^3\ g^{-1}$ for CS-T-2.5. This alteration in the aforementioned specific values, expressed per unit mass of the material, is attributed to a high density of TiO_2 that significantly contributes to the total mass of the composite material. Titania nanocrystals are the source of some of the surface area and porosity in the CS-T-2.5 material; however, this contribution is not sufficient enough to balance a substantial increase in the mass of the material. Furthermore, the formation of TiO_2 nanocrystals in the space between carbon particles (i.e., mesopores) reduces the total pore volume of the material by effectively excluding some space of pores. This excluded volume of mesopores relates to the decrease in their size from 6.1 nm for CS to 3.1 nm for CS-T-2.5. Subsequently, the aforementioned structural parameters change with removal of carbon from the CS-T-2.5 composite sample. The specific surface area of the carbon-free T-2.5 sample is further reduced to 130 $m^2\ g^{-1}$; however, this value is exceedingly high in comparison to the data available in the literature,[10−12] if highly crystalline, pure anatase structure of TiO_2 is taken into account (more details below). A similar evolution of successive isotherms is observed for the CS*-derived set of materials (Supprting Information Figure S4).

Table 2. Adsorption Parameters for the Materials Studied[a]

sample	S_{BET} ($m^2\ g^{-1}$)	V_t ($cm^3\ g^{-1}$)	V_{mi} ($cm^3\ g^{-1}$)	V_{me} ($cm^3\ g^{-1}$)	w_{mi} (nm)	w_{me} (nm)
CS	590	0.39	0.08	0.31	1.4	6.1
CS-T-2.5	240	0.25	0.05	0.2	1.5	3.1
T-2.5	130	0.27	0	0.27		6.4
CS*	580	0.36	0.08	0.28	1.2	4.5
CS*-T-0.7	390	0.32	0.07	0.25	1.4	
T*-0.7	42	0.14	0	0.14		6.9

[a] S_{BET}, BET specific surface area; V_t, single-point pore volume; V_{mi}, volume of micropores and small mesopores; V_{me}, volume of mesopores; w_{mi}, the pore width of micropores; w_{me}, the pore width of mesopores; w_{me} value at the maximum of PSD is not provided for CS*-T-0.7 because the PSD curve for this sample is flat.

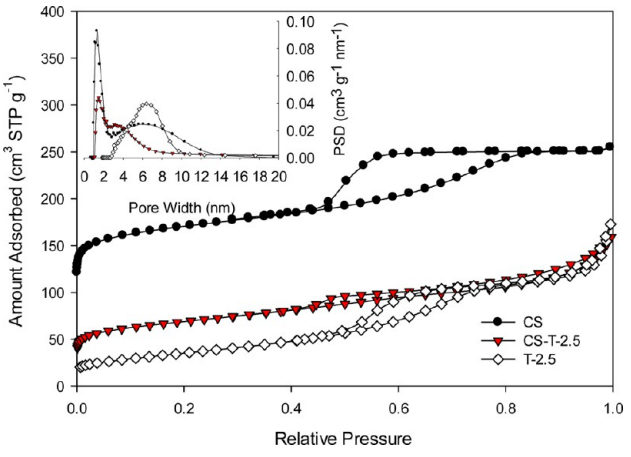

Figure 3. Nitrogen adsorption−desorption isotherms measured for CS, CS-T-2.5, and T-2.5 materials.

A comparison of CS and CS* materials (Supprting Information Figure S5), produced by varying the amount of polymer and using the same thermal treatment, shows that both materials exhibited mixed type I and IV isotherms with well-resolved hysteresis loop.[36] The latter indicates the presence of mesopores,[30] reflected respectively by large total pore volumes of 0.39 and 0.35 cm^3/g. The presence of micropores contributed to the high specific surface area of the CS and CS* samples,[30] reaching the values of 590 and 580 m^2/g accordingly. The isotherms of both samples coincide with each other in the initial (e.g., low-pressure) range, whereas their shapes in the mesopore range differ between the materials. The latter phenomenon is mainly due to the randomness of agglomeration of slightly different carbon spheres, which probably led to the observed variations in the pore size and mesopore volume of the CS and CS* samples, having mesopores of 6.1 nm and 4.5 nm and mesopore volumes of 0.31 $cm^3\ g^{-1}$ and 0.28 $cm^3\ g^{-1}$, respectively.

The composite materials (Supprting Information Figure S6) exhibit high specific surface areas too: 240 $m^2\ g^{-1}$ for CS-T-2.5 and 390 $m^2\ g^{-1}$ for CS*-T-0.7. As it was mentioned above, the specific quantities for titanium dioxide are smaller than those for carbons and carbon−titania composites because the density of TiO_2 is almost twice that of carbon. Therefore, the lower specific surface area of CS-T-2.5 as compared to CS*-T-0.7 can be explained by higher content of TiO_2 in the former. Consecutively, the CS*-T-0.7 material has higher total pore volume, 0.32 vs 0.25 $cm^3\ g^{-1}$, and more specifically, both the micro- and mesopore volumes as well. The micropore size, in the case of both materials, is the same (within an error margin) as the carbon particles from which the composites were derived, indicating that these particles are exclusively the source of microporosity in the composites studied. In contrast, the

mesopore size of composites decreased as compared to the carbon materials; CS-T-2.5 has mesopores of 3.1 nm, as estimated at the maximum of PSD, whereas the mesopore size of CS is 6.1 nm. The mesopore size of CS*-T-0.7, however, could not be estimated due to its shift towards smaller values and overlap with the peak referring to micropores.

Pure titania nanostructured materials were obtained from composite materials by carbon removal through calcination in air atmosphere. The process was intended to remove the carbon as well as to increase the crystallinity of the materials. For the purpose of comparison, Supprting Information Figure S7 shows adsorption isotherms for T-2.5 and T*-0.7. The observed morphological and structural differences between materials obtained by using different amounts of TIPO are clearly seen at this stage. With the carbon acting as the structure protecting medium, both materials featured relatively high specific surface area and porosity; however, after carbon removal the T-2.5 sample, obtained with larger amount of TIPO, exhibited higher values of both, the specific surface area and pore volume, 130 m^2 g^{-1} and 0.27 cm^3 g^{-1}, respectively. The corresponding values for T*-0.7 are 42 m^2 g^{-1} and 0.14 cm^3 g^{-1}, respectively. This proves that the porous structure of T-2.5, formed from larger amount of titania, is more stable than that of T*-0.7. The latter observation is additionally demonstrated by the fact that the T-2.5 material (130 m^2 g^{-1}) retained more than half of the specific surface area of its composite predecessor (240 m^2 g^{-1}), whereas T*-0.7 retained less than 11% of the composite surface area (42 vs 390 m^2 g^{-1}). A side-by-side comparison shows that the surface area of T*-0.7 constitutes only a third of the specific surface area of T-2.5. These values indicate that the thickness of the titania shell is not sufficient to be self-standing without the structural support provided by carbon in the case of a higher carbon to titania ratio.

Wide-angle X-ray diffraction (WAXRD) studies were performed in order to identify the crystalline phase and degree of crystallinity for the obtained materials. WAXRD spectra for the set of CS*, CS*-T-0.7, and T*-0.7 materials are shown in Figure 4 with the other samples demonstrating similar diffraction patterns (spectra not shown). The carbon spheres alone did not show any crystalline features, and a weak and broad peak around 25° comes from the amorphous carbon. In contrast, carbon−titania and pure titania materials showed clear crystalline features with major peaks at 25.4°, 38.0°, 48.0°, 54.7°, 63.1°. All these peaks correspond to the anatase crystal structure (ICDD PDF 01-071-1166), indicating that anatase was the only crystal phase present in both materials. These results demonstrate that titania was successfully transformed from its amorphous phase to anatase during thermal treatment, while the carbon scaffold provided the necessary support for this to occur without porous structure collapse. After calcination at 550 °C, conducted for the carbon removal, the resulting titania structures remained in the anatase phase with noticeable increase in crystallinity. This increase is reflected by more narrow and distinct diffraction peaks than those recorded for the composite materials. Analysis of crystallite size using Scherrer equation revealed that while titania in CS*-T-0.7 composite material has crystallite size of 7.1 nm, the size of crystallites in pure T*-0.7 material is 16.7 nm. The latter values show a good agreement with the values estimated based on TEM images. Moreover, a semi-quantitative analysis of the XRD data shows that the composite material had ca. one-third crystallinity of the corresponding pure titania material. The latter indicates how much titania materials are impacted by thermal treatment, which can be used to control the degree of crystallinity.

Thermogravimetric analysis (TGA) was used to determine thermal stability and composition of the carbon−titania materials. Thermogravimetric (TG) and differential TG (DTG) curves of CS-T-2.5 and CS*-T-0.7 materials are shown in Figure 5. Analysis of the TG data indicates that the

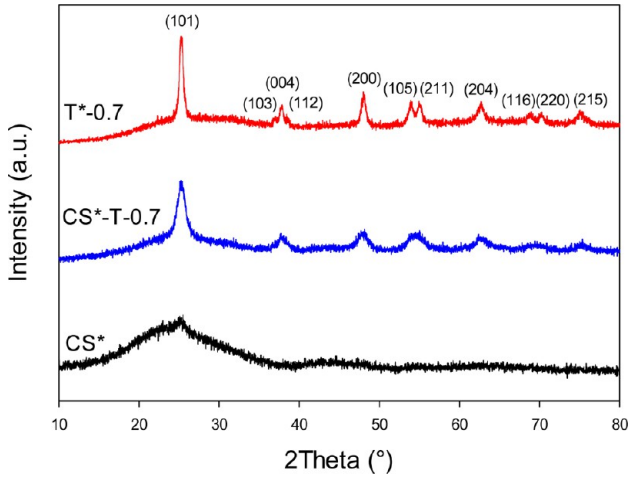

Figure 4. WAXRD patterns of CS*, CS*-T-0.7, and T*-0.7 materials.

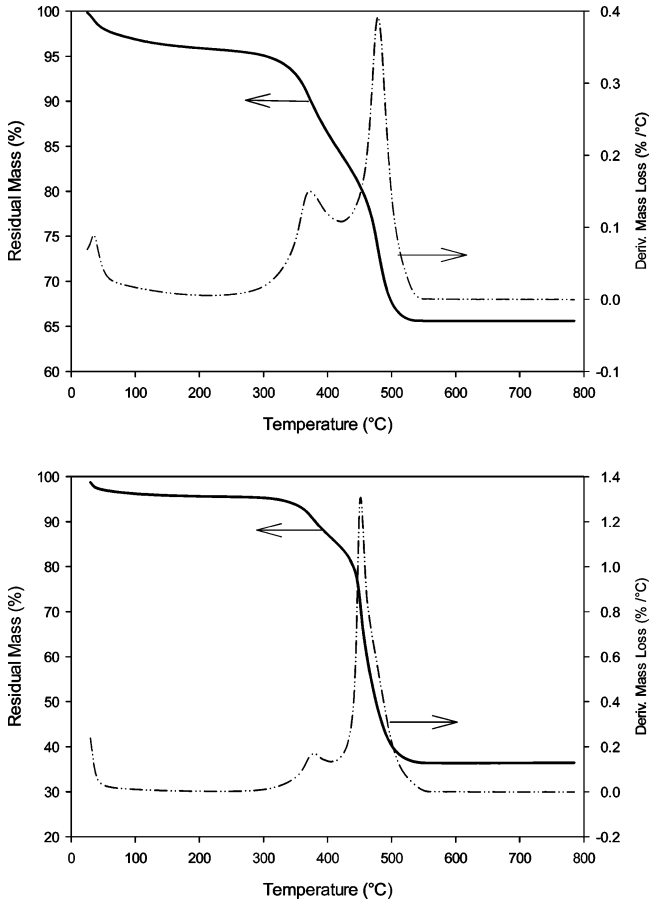

Figure 5. TG and DTG profiles of carbon−titania composite materials: CS-T-2.5 (A) and CS*-T-0.7 (B).

dx.doi.org/10.1021/am302691f | ACS Appl. Mater. Interfaces 2013, 5, 1948−1954

composites maintained thermal stability to approximately 350 °C in air atmosphere. The content of TiO_2 in the composite samples was established based on the residual mass after TG runs. The titania contents for CS-T-2.5 and CS*-T-0.7 composite materials were found to be 68% (w/w) and 38% (w/w), respectively. Those values differ to some extent from the predicted theoretical ones, which is most probably caused by partial precipitation of TiO_2 on the vessel walls during the microwave synthesis. Nevertheless, the proposed synthesis provides the ability to vary the amount of TiO_2 in the composite materials, which may be used to tailor properties of the composites as well as the derived materials for the desired applications.

4. CONCLUSIONS

Two sets of porous carbon−titania and highly crystalline nanostructured titania materials were synthesized and investigated. The study demonstrates the feasibility of microwave-assisted one-pot synthesis for the fabrication of the aforementioned materials with high specific surface area and well-developed porosity. The content of the composite materials can be adjusted based on the amount of titania precursor added during the synthesis. Titanium dioxide was established to be in anatase crystal phase in both the composite and pure titania materials. The degree of titania crystallization can be varied based on the applied thermal treatment. The importance of the carbon scaffold, which was provided by carbon particles to protect the porous structure of titania during thermal treatments, was clearly demonstrated. The composites, due to their high surface area and well developed porosity, have potential to be employed in the fields of lithium-based batteries, water treatment, and catalysis, while the pure titania materials, due to their high crystallinity, are highly potent for photocatalytic processes/devices, energy conversion, and photodegradation of pollutants. Further optimization of the synthesis conditions can be performed to gain the control over carbon particle sizes, porosity, and morphology of the resulting composite and titania materials.

■ ASSOCIATED CONTENT

Supporting Information

Additional SEM images and nitrogen adsorption−desorption isotherms for carbon particles, carbon−titania composites, and pure titania materials. This material is available free of charge via the Internet at http://pubs.acs.org.

■ AUTHOR INFORMATION

Corresponding Author

*E-mail: jaroniec@kent.edu. Fax: +1-330-672-3816. Tel: +1-330-672-3970.

Present Address

[†]A.P.: Department of Chemistry and Physics, High Point University, High Point, NC 27262, USA.

Notes

The authors declare no competing financial interest.

■ ACKNOWLEDGMENTS

The authors acknowledge the National Science Foundation for support of this research under CHE-1004987 (REU). The TEM data were obtained at the (cryo) TEM facility at the Liquid Crystal Institute, Kent State University, supported by the Ohio Research Scholars Program *Research Cluster on Surfaces in Advanced Materials*. The authors thank Dr. Min Gao for technical support with the TEM experiments.

■ REFERENCES

(1) Chaudhuri, R. G.; Paria, S. *Chem. Rev.* **2012**, *112*, 2373−2433.
(2) Carp, O.; Huisman, C.; Reller, A. *Prog. Solid State Chem.* **2004**, *32*, 33−177.
(3) Hashimoto, K.; Irie, H.; Fujishima, A. *Jpn. J. Appl. Phys.* **2005**, *44*, 8269−8285.
(4) Chen, X.; Shen, S.; Guo, L.; Mao, S. S. *Chem. Rev.* **2010**, *110*, 6503−6570.
(5) Martinu, L.; Poitras, D. *J. Vac. Sci. Technol., A* **2000**, *18*, 2619−2645.
(6) Su, X.; Wu, Q.; Zhan, X.; Wu, J.; Wei, S.; Guo, Z. *J. Mater. Sci.* **2012**, *47*, 2519−2534.
(7) Boucle, J.; Ackermann, J. *Polym. Int.* **2012**, *61*, 355−373.
(8) Brammer, K. S.; Frandsen, C. J.; Jin, S. *Trends Biotechnol.* **2012**, *30*, 315−322.
(9) Weir, A.; Westerhoff, P.; Fabricius, L.; Hristovski, K.; von Goetz, N. *Environ. Sci. Technol.* **2012**, *46*, 2242−2250.
(10) Ismail, A. A.; Bahnemann, D. W. *J. Mater. Chem.* **2011**, *21*, 11686−11707.
(11) Khataee, A.; Mansoori, G. A. In *Nanostructured Titanium Dioxide Materials*; World Scientific: Singapore, 2012.
(12) Chen, X.; Mao, S. S. *Chem. Rev.* **2007**, *107*, 2891−2959.
(13) Ao, Y.; Xu, J.; Fu, D.; Yuan, C. *Catal. Commun.* **2008**, *9*, 2574−2577.
(14) Zheng, R.; Meng, X.; Tang, F. *J. Solid State Chem.* **2009**, *182*, 1235−1240.
(15) Li, W.; Yang, J.; Wu, Z.; Wang, J.; Li, B.; Feng, S.; Deng, Y.; Zhang, F.; Zhao, D. *J. Am. Chem. Soc.* **2012**, *134*, 11864−11867.
(16) Zhuang, J.; Tian, Q.; Zhou, H.; Liu, Q.; Liu, P.; Zhong, H. *J. Mater. Chem.* **2012**, *22*, 7036−7042.
(17) Shi, J.; Zong, X.; Wu, X.; Cui, H.; Xu, B.; Wang, L.; Fu, M. *ChemCatChem* **2012**, *4*, 488−491.
(18) Wu, Z.; Dong, F.; Zhao, W.; Wang, H.; Liu, Y.; Guan, B. *Nanotechnology* **2009**, *20*, 235701−235710.
(19) Liu, R.; Ren, Y.; Shi, Y.; Zhang, F.; Zhang, L.; Tu, B.; Zhao, D. *Chem. Mater.* **2008**, *20*, 1140−1146.
(20) Froeschl, T.; Hoermann, U.; Kubiak, P.; Kucerova, G.; Pfanzelt, M.; Weiss, C. K.; Behm, R. J.; Huesing, N.; Kaiser, U.; Landfester, K.; Wohlfahrt-Mehrens, M. *Chem. Soc. Rev.* **2012**, *41*, 5313−5360.
(21) Zhu, G.; Wang, Y.; Xia, Y. *Energy Environ. Sci.* **2012**, *5*, 6652−6667.
(22) Zhang, W.; Zou, L.; Wang, L. *Appl. Catal., A* **2009**, *371*, 1−9.
(23) Huang, Z.; Xu, D.; Kang, F.; Hao, J. *New Carbon Mater.* **2004**, *19*, 229−238.
(24) Hsu, Y.; Lin, H.; Chen, C.; Liao, Y.; Yang, C. *J. Solid State Chem.* **2010**, *183*, 1917−1924.
(25) Jia, X.; He, W.; Zhang, X.; Zhao, H.; Li, Z.; Feng, Y. *Nanotechnology* **2007**, *18*, 75602−75609.
(26) Choma, J.; Jamiola, D.; Augustynek, K.; Marszewski, M.; Gao, M.; Jaroniec, M. *J. Mater. Chem.* **2012**, *22*, 12636−12642.
(27) Celer, E. B.; Jaroniec, M. *J. Am. Chem. Soc.* **2006**, *128*, 14408−14414.
(28) Brunauer, S.; Emmett, P. H.; Teller, E. *J. Am. Chem. Soc.* **1938**, *60*, 309−319.
(29) Gregg, S. J.; Sing, K. S. W. In *Adsorption, Surface Area and Porosity*; Academic Press: London, 1982.
(30) Kruk, M.; Jaroniec, M. *Chem. Mater.* **2001**, *13*, 3169−3183.
(31) Barrett, E. P.; Joyner, L. G.; Halenda, P. P. *J. Am. Chem. Soc.* **1951**, *73*, 373−380.
(32) Kruk, M.; Jaroniec, M.; Sayari, A. *Langmuir* **1997**, *13*, 6267−6273.
(33) Kruk, M.; Jaroniec, M.; Gadkaree, K. P. *J. Colloid Interface Sci.* **1997**, *192*, 250−256.
(34) Jaroniec, M.; Kruk, M.; Olivier, J. P. *Langmuir* **1999**, *15*, 5410−5413.

(35) Liu, J.; Qiao, S. Z.; Liu, H.; Chen, J.; Orpe, A.; Zhao, D.; Lu, G. Q. *Angew. Chem., Int. Ed.* **2011**, *50*, 5947−5951.
(36) Sing, K. S. W.; Everett, D. H.; Haul, R. A. W.; Moscou, L.; Pierotti, R. A.; Rouquerol, J.; Siemieniewska, T. *Pure Appl. Chem.* **1985**, *57*, 603−619.